Anisotropic flow in Cu + Au collisions at $\sqrt{s_{NN}} = 200$ GeV

Lie-Wen Chen[1,2] and Che Ming Ko[3]
[1]*Institute of Theoretical Physics, Shanghai Jiao Tong University, Shanghai 200240, China*
[2]*Center of Theoretical Nuclear Physics, National Laboratory of Heavy Ion Accelerator, Lanzhou 730000, China*
[3]*Cyclotron Institute and Physics Department, Texas A&M University, College Station, Texas 77843-3366, USA*
(Received 27 July 2005; published 27 January 2006)

The anisotropic flow of charged hadrons in asymmetric Cu + Au collisions at the Relativistic Heavy Ion Collider is studied in a multiphase transport model. Compared with previous results for symmetric Au + Au collisions, charged hadrons produced around midrapidity in asymmetric collisions are found to have a stronger directed flow v_1 and their elliptic flow v_2 is also more sensitive to the parton scattering cross section. Although higher order flows v_3 and v_4 are small at all rapidities, both v_1 and v_2 in these collisions are appreciable and show an asymmetry in forward and backward rapidities.

DOI: 10.1103/PhysRevC.73.014906 PACS number(s): 25.75.Ld, 24.10.Lx

I. INTRODUCTION

There have been extensive studies on the azimuthal anisotropy of hadron momentum distributions in the transverse plane perpendicular to the beam direction, particularly the elliptic flow v_2, in heavy-ion collisions at various energies [1]. The hadron transverse momentum anisotropy is generated by the pressure anisotropy in the initial compressed matter formed in noncentral heavy-ion collisions [2,3] and is sensitive to the properties of produced matter in these collisions. For heavy-ion collisions at the Relativistic Heavy Ion Collider (RHIC), it has been shown that this sensitivity exists not only in the larger elliptic flow [4–11] but also in smaller higher order anisotropic flows [12–18]. To investigate the influence of initial collision geometry on anisotropic flows in heavy-ion collisions, one usually varies the impact parameter of a collision or the atomic number of colliding nuclei [19]. Another possibility is to study asymmetric heavy-ion collisions with unequal mass nuclei as their initial collision geometry is different from that in collisions with equal-mass nuclei.

In the present work, we use a multiphase transport (AMPT) model, which includes both initial partonic and final hadronic interactions [20,21], to study the anisotropic flows v_1, v_2, v_3, and v_4 of charged hadrons in asymmetric Cu + Au collisions at $\sqrt{s} = 200A$ GeV at RHIC. Use is made of both the default version and the version with string melting, that is, a version allowing hadrons that are expected to be formed from initial strings to convert to their valence quarks and antiquarks [10,22,23]. The latter was able to explain the measured p_T dependence of v_2 and v_4 of midrapidity charged hadrons with a parton scattering cross section of about 10 mb whereas the default version seemed to give a better description of the anisotropic flows at large rapidities where the string degree of freedom dominates [24]. We find that charged hadrons produced around midrapidity in asymmetric Cu + Au collisions have a stronger directed flow v_1 and their elliptic flow is also more sensitive to the parton scattering cross section than those found previously in symmetric Au + Au collisions. Furthermore, both v_1 and v_2 of charged hadrons are asymmetric in the forward and backward rapidities. The higher order flows v_3 and v_4 are generally small, and their sensitivity to the parton scattering cross section is thus less clear.

This paper is organized as follows. In Sec. II, the AMPT model is briefly reviewed. Results on the pseudorapidity dependence of the anisotropic flows of charged hadrons are shown in Sec. III. The p_T dependence of the anisotropic flows of charged hadrons around midrapidity is studied in Sec. IV whereas that at large rapidities is shown in Sec. V. Finally, a brief summary is given in Sec. VI.

II. THE AMPT MODEL

The AMPT model [20,21,25–27] is a hybrid model that uses minijet partons from hard processes and strings from soft processes in the Heavy Ion Jet Interaction Generator (HIJING) model [28] as the initial conditions for modeling heavy-ion collisions at ultra-relativistic energies. The time evolution of resulting minijet partons is described by Zhang's parton cascade (ZPC) [29] model. At present, this model includes only parton-parton elastic scatterings with an in-medium cross section given by

$$\frac{d\sigma_p}{dt} \approx \frac{9\pi\alpha_s^2}{2}\left(1+\frac{\mu^2}{s}\right)\frac{1}{(t-\mu^2)^2}, \tag{1}$$

where the strong coupling constant α_s is taken to be 0.47, and s and t are usual Mandelstam variables. The effective screening mass μ depends on the temperature and density of the partonic matter but is taken as a parameter in ZPC for fixing the magnitude and angular distribution of the parton scattering cross section. After minijet partons stop interacting, they are combined with their parent strings, as in the HIJING model with jet quenching, to fragment into hadrons using the Lund string fragmentation model as implemented in the PYTHIA program [30]. Final-state scatterings among hadrons are then modeled by a relativistic transport (ART) model [31]. The default AMPT model [20] has been quite successful in describing measured rapidity distributions of charge particles, particle to antiparticle ratios, and spectra of low transverse momentum pions and kaons [21] in heavy-ion collisions at

the Super Proton Synchrotron (SPS) and RHIC. It has also been useful in understanding the production of J/ψ [25] and multistrange baryons [26] in these collisions.

Since the initial energy density in heavy-ion collisions at RHIC is much greater than the critical energy density at which the hadronic matter to quark-gluon plasma transition would occur [19,25,32], the AMPT model has been extended to convert initial excited strings into partons [10]. In this string-melting scenario, hadrons (mostly pions), which would have been produced from string fragmentation, are converted instead to valence quarks and/or antiquarks with current quark masses. Interactions among these partons are again described by the ZPC parton cascade model. Since inelastic scatterings are not included, only quarks and antiquarks from melted strings are present in the partonic matter. The transition from the partonic matter to the hadronic matter is achieved using a simple coalescence model, which combines the two nearest quark and antiquark into mesons and the three nearest quarks or antiquarks into baryons or antibaryons that are close to the invariant mass of these partons. The present coalescence model is thus somewhat different from the ones recently used extensively [33–36] for studying hadron production at intermediate transverse momenta. By using parton scattering cross sections of 6−10 mb, the AMPT model with string melting was able to reproduce both the centrality and transverse momentum (below 2 GeV/c) dependence of the elliptic flow [10] and pion interferometry [22] measured in Au + Au collisions at $\sqrt{s} = 130A$ GeV at RHIC [37,38]. It has also been used for studying the kaon interferometry [39] and charm flow [40] in these collisions. We note that these parton cross sections are significantly smaller than that needed to reproduce the parton elliptic flow from the hydrodynamic model [41]. The resulting hadron elliptic flows in the AMPT model with string melting are, however, amplified by modeling hadronization via quark coalescence [36], leading to a satisfactory reproduction of experimental data. As shown earlier in Refs. [42,43], the hadronization of the quark-gluon plasma leads in general to such acceleration at freeze-out.

III. PSEUDORAPIDITY DEPENDENCE OF ANISOTROPIC FLOWS

The anisotropic flows v_n of particles in heavy-ion collisions are the Fourier coefficients in the decomposition of their transverse momentum spectra in the azimuthal angle ϕ with respect to the reaction plane [44], that is,

$$E\frac{d^3N}{dp^3} = \frac{1}{2\pi}\frac{dN}{p_T dp_T dy}\left[1 + \sum_{n=1}^{\infty} 2v_n(p_T, y)\cos(n\phi)\right]. \quad (2)$$

Because of the symmetry $\phi \leftrightarrow -\phi$ in the collision geometry, sine terms do not appear in this expansion. Since the projectile and target sides of the reaction plane can in principle be identified experimentally, all isotropic flows v_n's are generally finite. Although in collisions with equal-mass nuclei the odd-order anisotropic flows of particles vanish as a result of the symmetry $(y, \phi) \to (-y, \phi + \pi)$ at midrapidity and midrapidity only, for collisions of asymmetric nuclei the odd flow components are finite at midrapidity also.

Anisotropic flows depend on both particle transverse momentum and rapidity, and for a given rapidity the anisotropic flows at transverse momentum p_T can be evaluated according to

$$v_n(p_T) = \langle \cos(n\phi) \rangle , \quad (3)$$

where $\langle \cdots \rangle$ denotes average over the azimuthal distribution of particles with transverse momentum p_T.

The anisotropic flows v_n can further be expressed in terms of single-particle averages:

$$v_1(p_T) = \left\langle \frac{p_x}{p_T} \right\rangle, \quad (4)$$

$$v_2(p_T) = \left\langle \frac{p_x^2 - p_y^2}{p_T^2} \right\rangle, \quad (5)$$

$$v_3(p_T) = \left\langle \frac{p_x^3 - 3p_x p_y^2}{p_T^3} \right\rangle, \quad (6)$$

$$v_4(p_T) = \left\langle \frac{p_x^4 - 6p_x^2 p_y^2 + p_y^4}{p_T^4} \right\rangle, \quad (7)$$

where p_x and p_y are, respectively, projections of particle momentum in and perpendicular to the reaction plane. Since the AMPT model also provides information on the spatial anisotropy of colliding nuclear matter, which is responsible for generating the momentum anisotropic flows, it is of interest to introduce the spatial anisotropic coefficient s_n by expressions similar to those for the anisotropic flows v_n but in terms of the spatial distributions of particles in the transverse plane.

In Figs. 1(a) and 1(b), we show the pseudorapidity dependence of v_1 and v_3, respectively, for charged hadrons from minimum bias events of Cu + Au collisions at $\sqrt{s} = 200A$ GeV by using the string-melting scenario with parton scattering cross

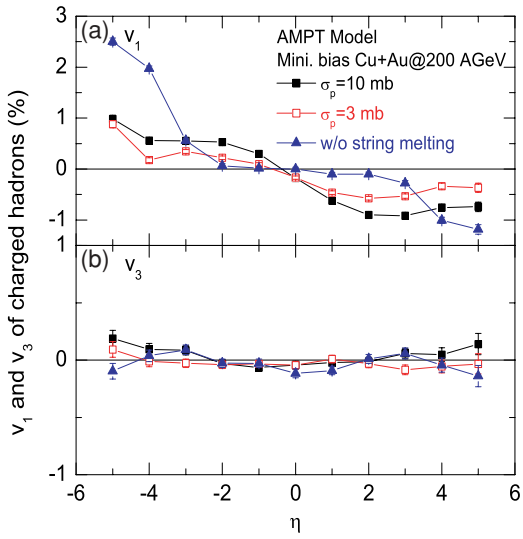

FIG. 1. (Color online) Pseudorapidity dependence of v_1(a) and v_3(b) for charged hadrons from minimum bias events of Cu + Au collisions at $\sqrt{s} = 200A$ GeV by using the string melting scenario with parton scattering cross sections $\sigma_p = 3$ (open squares) and 10 mb (solid squares) and the default AMPT model without string melting (solid triangles).

sections $\sigma_p = 3$ (open squares) and 10 mb (solid squares) and also the scenario without string melting (default AMPT model, solid triangles). Compared with the AMPT results shown in Fig. 2 of Ref. [24] for Au + Au collisions at the same c.m. energy per nucleon (where the string-melting scenario with a parton scattering cross section of 10 mb describes the experimental data around mid-rapidity from the STAR collaboration [16] very well), asymmetric Cu + Au collisions clearly display a stronger v_1 around mid-η in the AMPT model with string melting. Also, the pseudorapidity dependence of v_1 has a negative slope around mid-η and is sensitive to the parton scattering cross section. It is further seen from Fig. 1(a) that the p_T-integrated v_1 is very small around mid-η in the default AMPT model without string melting. In addition, v_1 displays an asymmetry in forward and backward rapidities around mid-η with the magnitude of v_1 at forward rapidity larger than that at backward rapidity. As shown later, this asymmetry is related to the different spatial deformation at forward and backward rapidities around mid-η. For the scenario without string melting, an even stronger asymmetry of v_1 in forward and backward rapidities is seen at larger pseudorapidity ($|\eta| \geqslant 3$), with the magnitude of v_1 at large backward pseudorapidity (Au-like rapidity) about a factor of 2 larger than that at large forward pseudorapidity (Cu-like rapidity). This result can be understood from the fact that hadronic degrees of freedom dominate at large pseudorapidities as the scenario without string melting has been shown in Ref. [24] to give a better description of the STAR data [16], and there are thus more hadrons and hadronic rescattering at the Au-like rapidity. We will return to this point later. However, the magnitude of the p_T-integrated v_3 is very small (less than 0.3%) in the whole pseudorapidity region for all three scenarios considered here.

The pseudorapidity dependence of v_2 and v_4 for charged hadrons from minimum bias events of Cu + Au collisions at $\sqrt{s} = 200A$ GeV is shown in Fig. 2 by using the same three scenarios as in Fig. 1. Similar to v_1 shown in Fig. 1, the elliptic flow v_2 displays a clear asymmetry in forward and backward rapidities around mid-η as well as at large pseudorapidity. In the case of the string-melting scenario with a parton scattering cross section of 10 mb, the value of v_2 around mid-η is about 3%. Compared with the v_2 value of about 4.5% around mid-η in Au + Au collisions at the same c.m. energy per nucleon shown in Fig. 3 of Ref. [24], the scaling of elliptic flow according to the reaction system size as proposed in Ref. [19] is also satisfied in asymmetric collisions. As in the case of v_3 shown in Fig. 1(b), the magnitude of the higher order p_T-integrated v_4 is also very small (less than 0.3%) in the whole pseudorapidity region for all three scenarios.

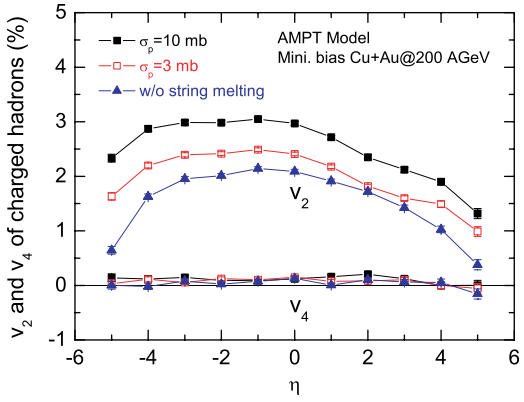

FIG. 2. (Color online) Same as Fig. 1 for v_2 and v_4.

IV. p_T DEPENDENCE OF ANISOTROPIC FLOWS AROUND MIDRAPIDITY

More detailed information on anisotropic flows can be obtained from the differential anisotropic flows (i.e., their p_T dependence). For hadrons produced around mid-η in heavy-ion collisions at RHIC, the partonic degree of freedom is expected to be important and the scenario with string melting describes the observed anisotropic flows of charged hadrons [24] very well. In Fig. 3, we show results obtained with the string-melting scenario on the p_T dependence of v_1, v_2, v_3, and v_4 for charged hadrons at forward mid-η ($0 < \eta < 1.2$, left panels) and backward mid-η ($-1.2 < \eta < 0$, right panels) from minimum bias events of Cu + Au collisions at $\sqrt{s} = 200A$ GeV. Both parton scattering cross sections $\sigma_p = 3$ (open squares) and 10 mb (solid squares) are used. The sensitivity to the parton cross section is clearly seen in v_2 and v_4 at both forward and backward mid-η. We note that the elliptic flow exhibits a stronger sensitivity to the parton cross section in asymmetric Cu + Au collisions than in symmetric Au + Au collisions. For example, the ratio of v_2 with $\sigma_p = 10$ mb to that with $\sigma_p = 3$ mb is about 1.4 in Cu + Au collisions but is reduced to about 1.2 in Au + Au collisions as given in

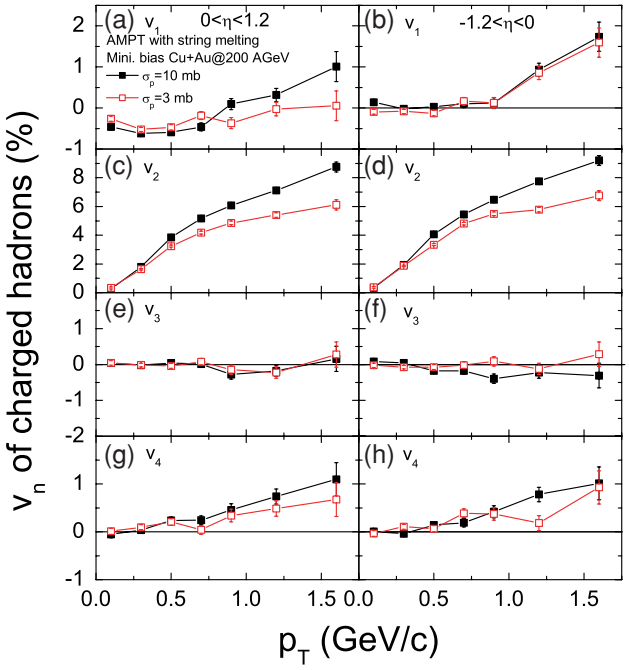

FIG. 3. (Color online) p_T dependence of v_1 [(a) and (b)], v_2 [(c) and (d)], v_3 [(e) and (f)], and v_4 [(g) and (h)] for charged hadrons at forward mid-η ($0 < \eta < 1.2$, left panels) and backward mid-η ($-1.2 < \eta < 0$, right panels) from minimum bias events of Cu + Au collisions at $\sqrt{s} = 200A$ GeV.

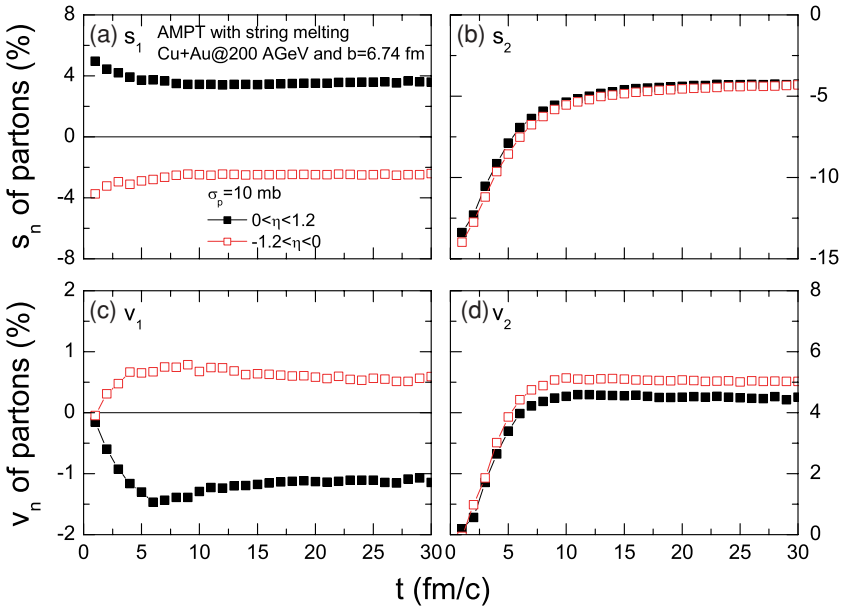

FIG. 4. (Color online) Time evolutions of s_1 (a), s_2 (b), v_1 (c), and v_2 (d) of partons at forward mid-η ($0 < \eta < 1.2$, solid squares) and backward mid-η ($-1.2 < \eta < 0$, open squares) from Cu + Au collisions at $\sqrt{s} = 200A$ GeV and $b = 6.74$ fm in the scenario of string melting with $\sigma_p = 10$ mb.

Fig. 2 of Ref. [17]. A similar conclusion is obtained for v_4. Sensitivities of the p_T dependence of v_1 at forward mid-η and v_3 at backward mid-η to the parton cross section are also seen.

Figure 3 also shows that the p_T dependence of v_1 at forward and backward mid-η exhibits very different behaviors. At forward mid-η, $v_1(p_T)$ is nonzero and changes from negative to positive values at a balance transverse momentum whereas $v_1(p_T)$ at backward mid-η is essentially zero at low p_T and becomes large and positive above about 0.8 GeV/c for both parton cross sections. As a result, the p_T-integrated v_1 of charged hadrons around mid-η displays the asymmetry in forward and backward rapidities shown in Fig. 1(a). For v_2, its value at backward mid-η is slightly larger than that at forward mid-η whereas the value of v_4 exhibits an opposite behavior. The difference between the p_T dependence of v_3 at forward and backward mid-η is, however, not so clear owing to their small values.

The asymmetry in forward and backward rapidities around mid-η observed in Fig. 3 can be better understood from the time evolutions of parton spatial deformation and anisotropic flows as the latter are transferred to those of hadrons when they are formed from quark and/or antiquark coalescence. Also, scatterings among hadrons, which are included in the AMPT model, do not have much effect on hadron anisotropic flows as a result of the small spatial anisotropy and low pressure in hadronic matter [10]. In Fig. 4, we show the time evolutions of s_1, s_2, v_1, and v_2 of partons at forward mid-η ($0 < \eta < 1.2$, solid squares) and backward mid-η ($-1.2 < \eta < 0$, open squares) from Cu + Au collisions at $\sqrt{s} = 200A$ GeV and $b = 6.74$ fm in the scenario of string melting with $\sigma_p = 10$ mb. We note that the impact parameter $b = 6.74$ fm corresponds to the same $b/b_{\max}$ as in Au + Au collisions at $b = 8$ fm, where $b_{\max}$ is the sum of the radii of colliding nuclei. Similar results for s_3, s_4, v_3, and v_4 are shown in Fig. 5.

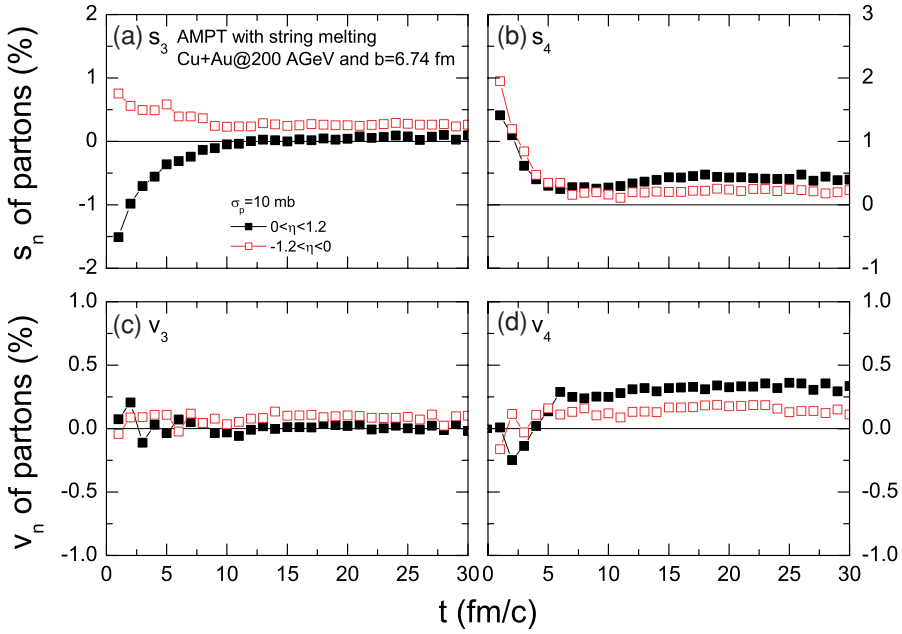

FIG. 5. (Color online) Same as Fig. 4 but for s_3 (a), s_4 (b), v_3 (c), and v_4 (d).

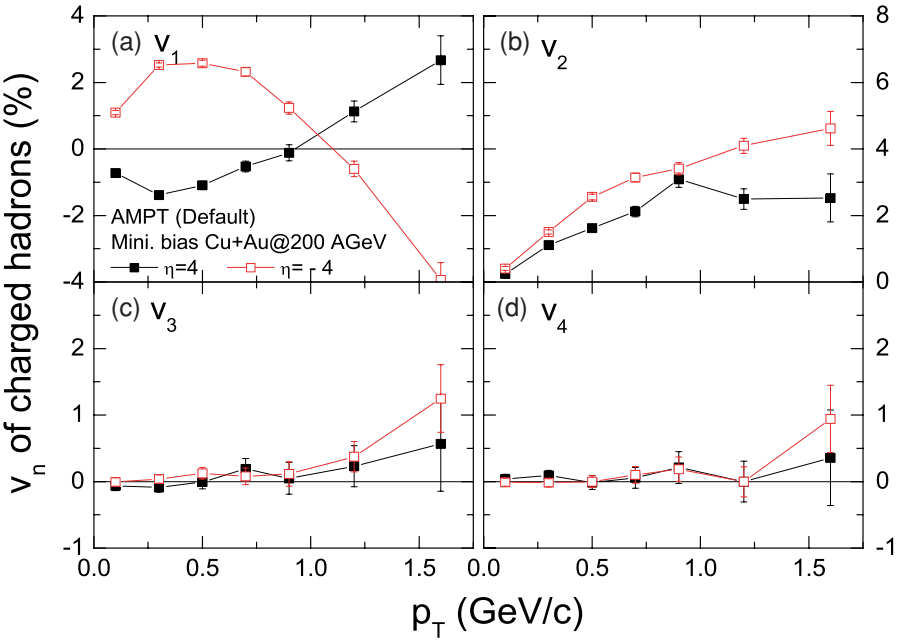

FIG. 6. (Color online) p_T dependence of v_1 (a), v_2 (b), v_3 (c), and v_4 (d) for charged hadrons at large forward pseudorapidity ($\eta = 4$, solid squares) and backward pseudorapidity ($\eta = -4$, open squares) from minimum bias events of Cu + Au collisions at $\sqrt{s} = 200A$ GeV.

It is seen from Fig. 4(a) that the strength of the spatial deformation coefficient s_1 is initially large and decreases with time. It reaches a saturation value at about 10 fm/c for partons at both forward and backward mid-η. The strength of s_1 at forward mid-η is, however, larger than that at backward mid-η, leading thus to a stronger v_1 at forward mid-η, as seen in Fig. 4(c) and also in Fig. 1(a). However, Fig. 4(b) shows that the strength of parton spatial elliptic deformation, s_2, is slightly larger at backward mid-η than at forward mid-η, resulting in a slightly stronger v_2 at backward mid-η, as is shown in Fig. 4(d) and also in Figs. 2 and 3. Therefore, the observed asymmetry of v_1 and v_2 in forward and backward rapidities around mid-η is due to an asymmetry in initial spatial deformation in asymmetric heavy-ion collisions.

From Fig. 5(a), we observe that the s_3 displays different time evolutions for partons at forward and backward mid-η and that its saturated value at backward mid-η is larger than that at forward mid-η. As a result, a stronger v_3 at backward mid-η as shown in Fig. 5(c) is seen. s_4 also displays different time evolutions for partons at forward and backward mid-η. Its saturated value is, however, larger at forward than at backward mid-η, leading to a stronger v_4 at forward mid-η, as shown in Fig. 5(d) and also in Fig. 3. However, because of its small value, the asymmetry in forward and backward rapidities is not so clear for the v_3 of charged hadrons around mid-η, as shown in Figs. 1(b) and 3.

V. p_T DEPENDENCE OF ANISOTROPIC FLOWS AT LARGE RAPIDITY

For hadrons at large rapidities ($|\eta| \geqslant 3$) in heavy-ion collisions at RHIC, the initial dynamics is expected to be dominated by the string degree of freedom as strings are produced later in time when the volume of the system is large and the energy density is low. Indeed, it has been shown that the default AMPT model in the scenario without string melting can describe simultaneously data on v_1 and v_2 at large pseudorapidity ($|\eta| \geqslant 3$) in Au + Au collisions at $\sqrt{s} = 200A$ GeV [24]. Therefore, it is of interest to study anisotropic flows at large rapidities in asymmetric Cu + Au collisions at RHIC based on the AMPT model without string melting. In Fig. 6, we show the predicted p_T dependence of v_1, v_2, v_3, and v_4 of charged hadrons at forward ($\eta = 4$, solid squares) and backward ($\eta = -4$, open squares) pseudorapidities from minimum bias events of Cu + Au collisions at $\sqrt{s} = 200A$ GeV. It is seen that the directed flow $v_1(p_T)$ shown in Fig. 6(a) exhibits a strong asymmetry in forward and backward rapidities, with charged hadrons at backward pseudorapidity having a much stronger $v_1(p_T)$ than that at forward pseudorapidity. Furthermore, v_1 at forward pseudorapidity changes from negative to positive values at a balance transverse momentum of about 0.8 GeV/c whereas v_1 at backward pseudorapidity changes from positive to negative values at a balance transverse momentum of about 1.2 GeV/c. A balance transverse momentum for v_1 has also been observed in symmetric Au + Au collisions, as shown in Fig. 4 of Ref. [24], and its existence has been attributed to the presence of transverse radial expansion [45].

A clear asymmetry of the elliptic flow v_2 in forward and backward rapidities is also seen in Fig. 6(b), with charged hadrons at backward pseudorapidity showing a stronger $v_2(p_T)$ than that at forward pseudorapidity. A similar asymmetry in forward and backward rapidities is observed in the higher order anisotropic flow $v_3(p_T)$ at higher p_T, as shown in Fig. 6(c). The higher order anisotropic flow $v_4(p_T)$ shown in Fig. 6(d) is essentially zero and it is not clear whether it has an asymmetry in forward and backward rapidities.

The observed strong asymmetry of charged hadron directed flow v_1 and elliptic flow v_2 in large forward and backward

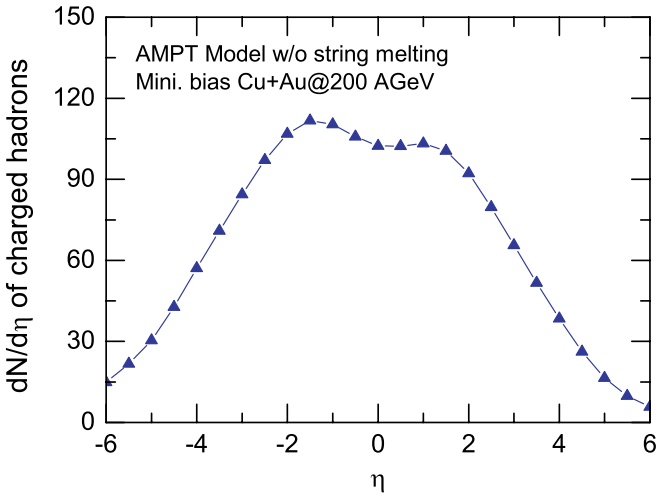

FIG. 7. (Color online) Charged hadron pseudorapidity density for minimum bias events of Cu + Au collisions at $\sqrt{s} = 200A$ GeV from the AMPT model in the scenario without string melting.

pseudorapidities may be related to the charged hadron pseudorapidity density, which is shown in Fig. 7 for minimum bias events of Cu + Au collisions at $\sqrt{s} = 200A$ GeV from the AMPT model in the scenario without string melting. It is seen that the charged hadron pseudorapidity density is asymmetric in forward and backward rapidities. Its value at backward pseudorapidity (Au-like rapidity) is larger than that at forward pseudorapidity (Cu-like rapidity), leading then to more hadronic rescattering and thus stronger v_1 and v_2 at backward pseudorapidity as observed here.

VI. SUMMARY

Using the AMPT model that includes both initial partonic and final hadronic interactions, we have studied the anisotropic flows v_1, v_2, v_3, and v_4 of charged hadrons in asymmetric Cu + Au collisions at RHIC. Comparing with AMPT results from symmetric Au + Au collisions shown in Refs. [17,24], we find that charged hadrons produced around midrapidity in asymmetric Cu + Au collisions display a stronger directed flow v_1 and their elliptic flow is also more sensitive to the parton cross section used in the parton cascade. Furthermore, although higher order v_3 and v_4 are small at all rapidities, both v_1 and v_2 in these collisions are appreciable and show an asymmetry in the forward and backward rapidities. This asymmetry is present even around midrapidity for v_1. Experimental verification of these predictions for asymmetric heavy-ion collisions at RHIC will be very useful in understanding the dynamics of asymmetric collisions. In addition, experimentally identifying the projectile and target sides of the reaction plane in symmetric collisions is rather difficult. This has led to a considerable delay in identifying the odd flow components, and the accuracy of the measurements of these harmonics still lags the accuracy and detail achieved in studies of elliptic flow. Study of collisions with asymmetric systems can contribute to a significant improvement in directed flow studies.

ACKNOWLEDGMENTS

This work was supported in part by the National Natural Science Foundation of China under Grant Nos. 10105008 and 10575071 (LWC) as well as by the U.S. National Science Foundation under Grant No. PHY-0457265 and the Welch Foundation under Grant No. A-1358 (CMK).

[1] W. Reisdorf and H. G. Ritter, Annu. Rev. Nucl. Part. Sci. **47**, 663 (1997).
[2] J. Barrette *et al*. (E877 Collaboration), Phys. Rev. Lett. **73**, 2532 (1994).
[3] H. Appelshauser *et al*. (NA49 Collaboration), Phys. Rev. Lett. **80**, 4136 (1998).
[4] J. Y. Ollitrault, Phys. Rev. D **46**, 229 (1992).
[5] H. Sorge, Phys. Lett. **B402**, 251 (1997); Phys. Rev. Lett. **78**, 2309 (1997); **82**, 2048 (1999).
[6] P. Danielewicz *et al*., Phys. Rev. Lett. **81**, 2438 (1998).
[7] B. Zhang, M. Gyulassy, and C. M. Ko, Phys. Lett. **B455**, 45 (1999).
[8] Y. M. Zheng, C. M. Ko, B. A. Li, and B. Zhang, Phys. Rev. Lett. **83**, 2534 (1999).
[9] M. Gyulassy, I. Vitev, and X. N. Wang, Phys. Rev. Lett. **86**, 2537 (2001).
[10] Z. W. Lin and C. M. Ko, Phys. Rev. C **65**, 034904 (2002).
[11] S. A. Voloshin, Nucl. Phys. **A715**, 379c (2003).
[12] P. F. Kolb, J. Sollfrank, and U. Heinz, Phys. Lett. **B459**, 667 (1999).
[13] D. Teaney and E. V. Shuryak, Phys. Rev. Lett. **83**, 4951 (1999).
[14] P. F. Kolb, J. Sollfrank, and U. Heinz, Phys. Rev. C **62**, 054909 (2000).
[15] P. F. Kolb, Phys. Rev. C **68**, 031902(R) (2003).
[16] J. Adams *et al*. (STAR Collaboration), Phys. Rev. Lett. **92**, 062301 (2004).
[17] L. W. Chen, C. M. Ko, and Z. W. Lin, Phys. Rev. C **69**, 031901(R) (2004).
[18] P. Kolb, L. W. Chen, V. Greco, and C. M. Ko, Phys. Rev. C **69**, 051901(R) (2004).
[19] L. W. Chen and C. M. Ko, Phys. Lett. B (2006), in press; nucl-th/0505044.
[20] B. Zhang, C. M. Ko, B. A. Li, and Z. Lin, Phys. Rev. C **61**, 067901 (2000).
[21] Z. W. Lin, S. Pal, C. M. Ko, B. A. Li, and B. Zhang, Phys. Rev. C **64**, 011902(R) (2001); Nucl. Phys. **A698**, 375 (2002).
[22] Z. W. Lin, C. M. Ko, and S. Pal, Phys. Rev. Lett. **89**, 152301 (2002).
[23] C. M. Ko, Z. W. Lin, and S. Pal, Heavy Ion Phys. **17**, 219 (2003).
[24] L. W. Chen, V. Greco, C. M. Ko, and P. F. Kolb, Phys. Lett. **B605**, 95 (2005).
[25] B. Zhang, C. M. Ko, B. A. Li, Z. Lin, and B. H. Sa, Phys. Rev. C **62**, 054905 (2000); B. Zhang, C. M. Ko, B. A. Li, Z. W. Lin, and S. Pal, *ibid*. **65**, 054909 (2002).
[26] S. Pal, C. M. Ko, and Z. W. Lin, Nucl. Phys. **A730**, 143 (2004).
[27] Z. W. Lin, C. M. Ko, B. A. Li, B. Zhang, and S. Pal, Phys. Rev. C **72**, 064901 (2005).

[28] X. N. Wang and M. Gyulassy, Phys. Rev. D **44**, 3501 (1991).
[29] B. Zhang, Comput. Phys. Commun. **109**, 193 (1998).
[30] T. Sjostrand, Comput. Phys. Commun. **82**, 74 (1994).
[31] B. A. Li and C. M. Ko, Phys. Rev. C **52**, 2037 (1995); B. A. Li, A. T. Sustich, B. Zhang, and C. M. Ko, Int. J. Phys. E **10**, 267 (2001).
[32] D. Kharzeev and M. Nardi, Phys. Lett. **B507**, 121 (2001).
[33] V. Greco, C. M. Ko, and P. Lévai, Phys. Rev. Lett. **90**, 202302 (2003); Phys. Rev. C **68**, 034904 (2003).
[34] R. C. Hwa and C. B. Yang, Phys. Rev. C **67**, 034902 (2003); **67** 064902 (2003).
[35] R. J. Fries, B. Müller, C. Nonaka, and S. A. Bass, Phys. Rev. Lett. **90**, 202303 (2003); Phys. Rev. C **68**, 044902 (2003).
[36] D. Molnar and S. A. Voloshin, Phys. Rev. Lett. **91**, 092301 (2003).
[37] K. H. Ackermann *et al*. (STAR Collaboration), Phys. Rev. Lett. **86**, 402 (2001).
[38] C. Adler *et al*. (STAR Collaboration), Phys. Rev. Lett. **87**, 082301 (2001).
[39] Z. W. Lin and C. M. Ko, J. Phys. G **30**, S263 (2004).
[40] B. Zhang, L. W. Chen, and C. M. Ko, Phys. Rev. C **72**, 024906 (2005).
[41] D. Molnar and P. Huovinen, Phys. Rev. Lett. **94**, 012302 (2005).
[42] T. Csorgo and L. P. Csernai, Phys. Lett. **B333**, 494 (1994).
[43] C. Anderlik *et al*., Phys. Rev. C **59**, 3309 (1999).
[44] A. M. Poskanzer and S. A. Voloshin, Phys. Rev. C **58**, 1671 (1998).
[45] S. A. Voloshin, Phys. Rev. C **55**, R1630 (1997).